Analytical expressions of incompatibility stresses at $\Sigma 3$ 111 twin boundaries and consequences on single-slip promotion parallel to twin plane

Thiebaud Richeton, I. Tiba, Stéphane Berbenni, O. Bouaziz

Philosophical Magazine
Vol. 95, No. 1, 2015, 12–31

RESEARCH ARTICLE

Analytical expressions of incompatibility stresses at $\Sigma 3 < 111 >$ twin boundaries and consequences on single slip promotion parallel to twin plane

T. Richeton[a*], I. Tiba[a,b], S. Berbenni[a], and O. Bouaziz[a]

[a]*Laboratoire d'Etude des Microstructures et de Mécanique des Matériaux (LEM3), UMR 7239, CNRS / Université de Lorraine, Ile du Saulcy, 57045 Metz, France*; [b]*Chair of Experimental Methods in Materials Science, Saarland University, D-66041 Saarbrcken, Germany*

(*v4.5 released May 2014*)

Strong incompatibility stresses may develop at grain or twin boundaries because of elastic and plastic anisotropies. Their knowledge at $\Sigma 3 < 111 >$ twin boundaries may be of interest for a better understanding of the mechanical behaviour of f.c.c. materials that can display lamellar twin structures such as TWIP steels or general nanotwinned materials. In this paper, incompatibility stresses arising at general twin boundaries are explicitly derived for a given twin volume fraction. They are deduced from the solutions of the general infinite bicrystal, which is equivalent to a periodic layered structure. In the case of pure elasticity and $\Sigma 3 < 111 >$ twin boundaries, the result is of remarkable simplicity. The incompatibility stress field reduces to a shear stress acting upon a plane orthogonal to twin plane. Simple analytical expressions of the resolved shear stresses are also determined according to the twin boundary orientation, the twin volume fraction and the elastic anisotropy factor. Such expressions allow performing a comprehensive study of slip initiation. In particular, there exists a large physical domain, depending on the three above parameters, where simultaneous slip parallel to twin plane in the parent and in the twin is greatly promoted. There is also a restricted domain where simultaneous single slip parallel to twin plane is promoted. The conditions for these promotions are realistic considering the literature data on TWIP steels. The present results hence support the high ductility and strong contribution of kinematic hardening observed in TWIP steels and agree with composite hardening models with single and multislip deforming grains.

Keywords: twinning; incompatibility stress; anisotropic elasticity; plasticity; TWIP; grain boundary engineering

1. Introduction

In polycrystals, incompatibility stresses arise due to the interaction of differently oriented adjacent grains that deform in an anisotropic way. For the same reason, the presence of twins inside grains induce also incompatibility stresses. These latter can be very strong and modify significantly the inter-granular stress heterogeneity. A well-known example is the role of twin boundaries in face-centred cubic (f.c.c.) materials as preferred sites for crack nucleation during high cycle fatigue (see [1–6] as a non-exhaustive list of examples). This phenomenon may appear unexpected at first view since twin boundaries have the lowest interfacial energy among all

*Corresponding author. Email: thiebaud.richeton@univ-lorraine.fr

grain boundaries in f.c.c. crystals. The general common explanation is that elastic anisotropy causes stress concentrations next to twin boundaries that promote earlier plastic strain. Numerous fatigue experiments were conducted to study this phenomenon, notably in copper [1, 2] and in austenitic steels [4–6] which show high values of their elastic anisotropy factor $A = \frac{2(s_{11}-s_{12})}{s_{44}}$ (s_{11}, s_{12} and s_{44} being the cubic elastic compliances, $A = 3.26$ for copper and $A \simeq 3.4$ for austenitic steels [7]). Under low cycle fatigue tests, the preferential role of twin boundaries to initiate fatigue cracking is much less evident [8]. It actually depends closely on crystallographic orientations, material stacking fault energy and plastic strain amplitude.

Incompatibility stresses that arise due to elastic mismatch at an interface can be estimated by finite element simulations (e.g., [9, 10]) but also thanks to simplified analytical models that assume piecewise uniform elastic fields. This kind of analytical model was initially proposed by Gemperlova et al. [11]. It applies in the bulk and appears in the form of a linear system of equations. A similar model was later used by Peralta et al. [12] and Blochwitz et al. [6] to study the role of texture on the fatigue behaviour of f.c.c. twin boundaries. In a proceeding paper, Neumann pointed out that in the case of f.c.c. twin boundaries, such model can be solved explicitly, using a mathematical software, and lead to remarkable simple solutions [13]. This important result seems however to have remained partly unknown from the community. In the present paper, these remarkable simple solutions are retrieved starting from the expressions of incompatibility stresses in an infinite bicrystal which were recently derived in explicit forms for the general case [14]. These solutions include the effects of plastic strains and are now given for any volume fraction of the component crystals (Section 3). Simplifications arising due to the twin symmetry (type I or II) are then first highlighted (Section 4) before handling in detail the case of f.c.c. twin boundaries (Section 5). In this last case, simple analytical expressions of the resolved shear stresses on f.c.c. slip systems are also given considering uniaxial loading. These expressions allow performing a comprehensive study of slip initiation at f.c.c. twin boundaries (Section 6).

In addition to fatigue resistance, the knowledge of incompatibility stresses at f.c.c. twin boundaries may be of interest for a better understanding of the mechanical behaviour of f.c.c. materials that can display lamellar twin structures. Lamellar twin structures can be encountered in twinning-induced plasticity (TWIP) steels or in general nanotwinned materials with a high density of twin boundaries. Such materials are actually quite promising since they exhibit greatly enhanced strength and very good ductility and toughness compared to ultra-fine or nano-grained materials [15, 16]. For instance, Pan et al. recently synthesized polycrystalline columnar-grained bulk Cu samples that contain preferentially oriented nanoscale twins by means of direct current electrodeposition and found an enhanced fatigue limit [17]. Their sample contained high densities of parallel growth twin lamellae with an average twin thickness of 78 nm. Concerning TWIP steels, images of the deformation structure reveal that a majority of grains contains very thin parallel twins ($< 100nm$) [18–20]. Multiple twinning systems may also be active and form, as a result, an intersecting layered substructure. Besides, it is often suggested that in heavily twinned grains, slip occurs predominantly parallel to the active twin plane since dislocations movement in other slip planes is hindered by twin boundaries. This suggestion is in particular recommended in order to capture texture evolution [20, 21]. One purpose of the present study is thus to highlight the role of elastic anisotropy on the potential promotion of slip on planes parallel to twin plane. This issue is handled in Section 6 through different numerical applications. The results are then discussed in Section 7 in relation with experimental data of

the literature. Notation conventions are settled in forthcoming Section 2.

2. Notation and reduction conventions

A bold symbol denotes a tensor. The symbol $\cdot$ represents tensor multiplication and a : the contracted product between two tensors. If $\mathbf{C}$ is a fourth-order tensor and $\mathbf{A}$ a second-order tensor, we have in rectangular Cartesian coordinates $(\mathbf{C} : \mathbf{A})_{ij} = C_{ijkl}A_{kl}$. Throughout the article, the contracted Voigt notation [22] ($11 \rightarrow 1, 22 \rightarrow 2, 33 \rightarrow 3, 23 \rightarrow 4, 31 \rightarrow 5, 12 \rightarrow 6$) is actually adopted concerning operations on fourth and second-order tensors. The contracted product between tensors $\mathbf{C}$ and $\mathbf{A}$ is then written as $(\mathbf{C} : \mathbf{A})_p = C_{pq}A_q$ where p and q take values ranging from 1 to 6. For consistency, an engineering convention is considered for strain components, i.e. $\varepsilon_4 = 2\varepsilon_{23}, \varepsilon_5 = 2\varepsilon_{31}, \varepsilon_6 = 2\varepsilon_{12}$, and the Hooke's law in matrix notation is given as

$$\begin{bmatrix} \varepsilon_1^e \\ \varepsilon_2^e \\ \varepsilon_3^e \\ \varepsilon_4^e \\ \varepsilon_5^e \\ \varepsilon_6^e \end{bmatrix} = \begin{bmatrix} s_{11} & s_{12} & s_{13} & s_{14} & s_{15} & s_{16} \\ s_{12} & s_{22} & s_{23} & s_{24} & s_{25} & s_{26} \\ s_{13} & s_{23} & s_{33} & s_{34} & s_{35} & s_{36} \\ s_{14} & s_{24} & s_{34} & s_{44} & s_{45} & s_{46} \\ s_{15} & s_{25} & s_{35} & s_{45} & s_{55} & s_{56} \\ s_{16} & s_{26} & s_{36} & s_{46} & s_{56} & s_{66} \end{bmatrix} \begin{bmatrix} \sigma_1 \\ \sigma_2 \\ \sigma_3 \\ \sigma_4 \\ \sigma_5 \\ \sigma_6 \end{bmatrix} \tag{1}$$

where ε_i^e are the elastic strains and s_{ij} are the components of the elastic compliances tensor that include the multiplying factors of 2 and 4 [22].

3. Incompatibility stresses for any infinite bicrystal with planar boundary

A fixed infinite planar interface separating two crystals is considered in a continuous medium, with unit normal vector $\mathbf{n}$ oriented from crystal I to crystal II along the x_2 direction (Figure 1). The volume fractions of crystal I and II in the infinite medium are denoted f^I and f^{II}. This bicrystal is subjected to far-field tractions on its fictitious external boundary, $\mathbf{T} = \mathbf{\Sigma} \cdot \mathbf{n}_s$ where the applied stress $\mathbf{\Sigma}$ is assumed macroscopically homogeneous and $\mathbf{n}_s$ stands for the outward normal. Elastic compliances $\mathbf{s}$ and plastic strains $\boldsymbol{\varepsilon}^{\mathbf{p}}$ are assumed to be piecewise uniform, i.e. uniform within each component crystal. The superscript I denotes fields in crystal I ($x_2 < 0$) and the superscript II fields in crystal II ($x_2 > 0$). The jump of a mechanical or a material property field $\mathbf{g}$ at the interface oriented by $\mathbf{n}$ is denoted $[\mathbf{g}] = \mathbf{g}^{\mathbf{II}}(x_2 \rightarrow 0^+) - \mathbf{g}^{\mathbf{I}}(x_2 \rightarrow 0^-)$. By extension, for a piecewise uniform field $\mathbf{w}$, the difference between the fields in crystals II and I is written as $[\mathbf{w}] = \mathbf{w}^{\mathbf{II}} - \mathbf{w}^{\mathbf{I}}$. Recently, stress solutions of this general elastic-plastic problem were explicitly derived in [14] and in [23] considering the linear theory of small perturbations, strains compatibility and balance of stresses without body force. As a result, the stress tensor in crystal II is expressed as

$$\boldsymbol{\sigma}^{\mathbf{II}} = \mathbf{B}^{\mathbf{II}} : \mathbf{\Sigma} + \boldsymbol{\sigma}^{\mathbf{resII}} = \mathbf{B}^{\mathbf{II}} : \mathbf{\Sigma} + \mathbf{F}^{\mathbf{II}} : [\boldsymbol{\varepsilon}^{\mathbf{p}}] \tag{2}$$

where $\mathbf{B}^{\mathbf{II}}$ is the elastic stress concentration tensor and $\mathbf{F}^{\mathbf{II}}$ is the stress influence tensor [14, 24, 25]. The second term of this expression, $\boldsymbol{\sigma}^{\mathbf{resII}} = \mathbf{F}^{\mathbf{II}} : [\boldsymbol{\varepsilon}^{\mathbf{p}}]$, is the residual stress tensor. It turns out that the tensors $\mathbf{B}^{\mathbf{II}}$ and $\mathbf{F}^{\mathbf{II}}$ are actually linked

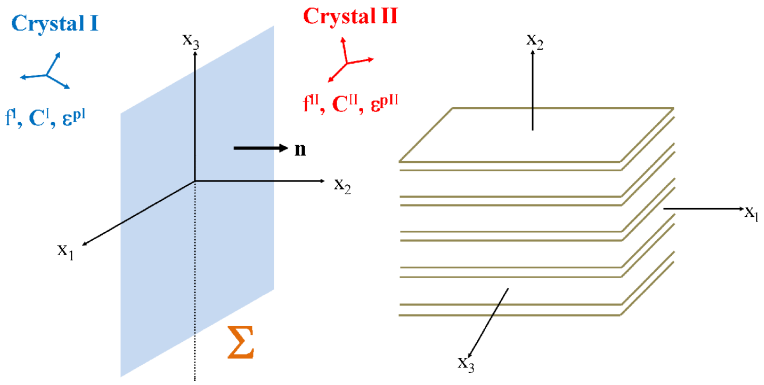

Figure 1. Infinite bicrystal with a planar boundary (left). Periodic layered structure (right).

by the relation $B^{II}_{ij} = \delta_{ij} + F^{II}_{ik}[s_{kj}]$ where δ_{ij} is the Kronecker delta. Hence, $\boldsymbol{\sigma}^{\mathbf{II}}$ can also be written as

$$\boldsymbol{\sigma}^{\mathbf{II}} = \boldsymbol{\Sigma} + \boldsymbol{\sigma}^{\mathbf{incII}} = \boldsymbol{\Sigma} + \mathbf{F}^{\mathbf{II}} : ([\mathbf{s}] : \boldsymbol{\Sigma} + [\boldsymbol{\varepsilon}^{\mathbf{p}}]) \tag{3}$$

The second term of the above expression, $\boldsymbol{\sigma}^{\mathbf{incII}} = \mathbf{F}^{\mathbf{II}} : ([\mathbf{s}] : \boldsymbol{\Sigma} + [\boldsymbol{\varepsilon}^{\mathbf{p}}])$, now represents what is usually denominated as the incompatibility stress tensor. The stress tensor in crystal I writes in a similar manner with $\mathbf{F}^{\mathbf{I}} = -\frac{f^{II}}{f^I}\mathbf{F}^{\mathbf{II}}$. Besides, in order to track expressions as concise as possible, the tensor $\boldsymbol{\sigma}^{\mathbf{inc}\star}$ is introduced. It is related to the incompatibility stress tensors in crystals I and II as

$$\boldsymbol{\sigma}^{\mathbf{incI}} = -f^{II}\boldsymbol{\sigma}^{\mathbf{inc}\star} \ , \ \boldsymbol{\sigma}^{\mathbf{incII}} = f^I\boldsymbol{\sigma}^{\mathbf{inc}\star} \tag{4}$$

The notations below are also adopted

$$\begin{aligned} &[\boldsymbol{\varepsilon}^\star] = [\mathbf{s}] : \boldsymbol{\Sigma} + [\boldsymbol{\varepsilon}^{\mathbf{p}}] \\ &\tilde{\mathbf{s}} = f^{II}\mathbf{s}^{\mathbf{I}} + f^I\mathbf{s}^{\mathbf{II}} = \mathbf{s}^{\mathbf{I}} + f^I[\mathbf{s}] \\ &\mathbf{G} = \frac{1}{f^I}\mathbf{F}^{\mathbf{II}} = -\frac{1}{f^{II}}\mathbf{F}^{\mathbf{I}} \end{aligned} \tag{5}$$

in order to write the stresses in crystals I and II in the following way

$$\boldsymbol{\sigma}^{\mathbf{I}} = \boldsymbol{\Sigma} - f^{II}\boldsymbol{\sigma}^{\mathbf{inc}\star} \ , \ \boldsymbol{\sigma}^{\mathbf{II}} = \boldsymbol{\Sigma} + f^I\boldsymbol{\sigma}^{\mathbf{inc}\star} \ \text{ with } \boldsymbol{\sigma}^{\mathbf{inc}\star} = \mathbf{G}[\boldsymbol{\varepsilon}^\star] \tag{6}$$

where the non-zero components of the symmetric tensor $\mathbf{G}$ are explicitly given below

$$\begin{aligned} &G_{11} = \left(\tilde{s}_{33}\tilde{s}_{55} - \tilde{s}^2_{35}\right)/D \ , \ G_{13} = \left(\tilde{s}_{15}\tilde{s}_{35} - \tilde{s}_{13}\tilde{s}_{55}\right)/D \ , \\ &G_{33} = \left(\tilde{s}_{11}\tilde{s}_{55} - \tilde{s}^2_{15}\right)/D \ , \ G_{15} = \left(\tilde{s}_{13}\tilde{s}_{35} - \tilde{s}_{15}\tilde{s}_{33}\right)/D \ , \\ &G_{55} = \left(\tilde{s}_{11}\tilde{s}_{33} - \tilde{s}^2_{13}\right)/D \ , \ G_{35} = \left(\tilde{s}_{13}\tilde{s}_{15} - \tilde{s}_{35}\tilde{s}_{11}\right)/D \ , \\ &\text{with } D = \tilde{s}_{11}\tilde{s}^2_{35} + \tilde{s}_{33}\tilde{s}^2_{15} + \tilde{s}_{55}\tilde{s}^2_{13} - \tilde{s}_{11}\tilde{s}_{33}\tilde{s}_{55} - 2\tilde{s}_{13}\tilde{s}_{15}\tilde{s}_{35} \end{aligned} \tag{7}$$

All the other components of $\mathbf{G}$ are zero, i.e. $G_{AA} = G_{AP} = 0$ with P the plane

components $(1,3,5)$ and A the anti-plane components $(2,4,6)$. Hence, it must be noted that the anti-plane components of $[\boldsymbol{\varepsilon}^\star]$ do not induce any incompatibility stress and that the anti-plane components of the incompatibility stress tensors are zero since tractions on the interface must be continuous

$$\sigma_A^{inc\star} = 0 \tag{8}$$

The above closed-form solutions show coupled effects of plastic incompatibilities and elastic mismatch at the interface. In the first place, they were derived some years ago in the particular case of homogeneous isotropic elasticity [26, 27]. Stress solutions in anisotropic elasticity were also previously given by different authors but, as mentioned in the Introduction, only in the form of a linear system of equations and for a same volume fraction of the component crystals [6, 11, 12, 28]. In [14], it was verified that the general solutions given by Equations 6 and 7 match perfectly the stress outputs of Finite Elements simulations when the latter are performed on a bicrystal with periodic boundary conditions. Peralta et al. [29] considered the case of finite bicrystals and showed that the average values of stresses given by a Finite Element model are in reasonable agreement with these analytical solutions.

Besides, it is noteworthy that the previous stress expressions established for an infinite bicrystal also apply to the case of a periodic layered composite with uniform elasticity and plasticity in each phase (see Figure 1). Indeed, the field equations of a one-rank laminate structure (compatibility conditions, stress equilibrium, problem's invariance) remain the same as those of the infinite bicrystal (for details about these equations, see [14, 23] for bicrystals and [24, 25, 30] for laminate structures). Hence, $\boldsymbol{\sigma}^{\mathbf{I}}$ and $\boldsymbol{\sigma}^{\mathbf{II}}$ are also the respective stress tensors in each phase of a periodic layered structure.

4. Incompatibility stresses in case of twin symmetry

In this section, the planar interfaces of Figure 1 are assumed to be twin boundaries with I the parent phase and II the twin phase. The process of twinning is accomplished by a simple shear of a crystal region, so that the new twin lattice becomes the mirror image of the original parent lattice [31]. In reality, twins have finite dimensions and the twinning shear distortion itself induce incompatibility stresses. However, within the present configuration of lamellar twin structure (Figure 1b), the twinning shear does not induce any incompatibility stress since it occurs in the interface plane (only anti-plane components of $[\boldsymbol{\varepsilon}^\star]$ are at stake, cf. Equations 6 and 7). Moreover, because of tractions continuity, there are no incompatibility stress acting on the twin plane (cf. Equation 8). Then, $(\mathbf{e_1^*}, \mathbf{e_2^*}, \mathbf{e_3^*})$ is defined as the basis vectors of an orthonormal frame attached to the twin boundary. $\mathbf{e_1^*}$ and $\mathbf{e_2^*}$ are collinear, respectively, to $\boldsymbol{\eta_1}$, the twinning shear direction, and to $\mathbf{n}^{\mathbf{K_1}}$, the normal to the $\mathbf{K_1}$ plane where the twinning shear occurred. In the rest of the paper, s_{ij}^* will designate the elastic compliances of crystal I in the twin boundary frame, whereas s_{ij} will designate the elastic compliances in the single crystal frame.

4.1. *Type I twins*

For type I twinning, the orientation of the twin lattice relative to the parent one corresponds to a 180° rotation around $\mathbf{n}^{\mathbf{K_1}}$ [31]. Hence, in the twin boundary

frame, the elastic compliance tensor of crystal II (i.e., the twin phase), $\mathbf{S^{II}}$, is deduced from the elastic compliance tensor of crystal I (i.e., the parent phase), $\mathbf{S^{I}} = \mathbf{s}^*$, by a 180 ° rotation around $\mathbf{e_2^*}$. As a result of this rotation, $\mathbf{S^{II}}$ reads

$$\mathbf{S^{II}} = \begin{bmatrix} s_{11}^* & s_{12}^* & s_{13}^* & -s_{14}^* & s_{15}^* & -s_{16}^* \\ s_{12}^* & s_{22}^* & s_{23}^* & -s_{24}^* & s_{25}^* & -s_{26}^* \\ s_{13}^* & s_{23}^* & s_{33}^* & -s_{34}^* & s_{35}^* & -s_{36}^* \\ -s_{14}^* & -s_{24}^* & -s_{34}^* & s_{44}^* & -s_{45}^* & s_{46}^* \\ s_{15}^* & s_{25}^* & s_{35}^* & -s_{45}^* & s_{55}^* & -s_{56}^* \\ -s_{16}^* & -s_{26}^* & -s_{36}^* & s_{46}^* & -s_{56}^* & s_{66}^* \end{bmatrix} \tag{9}$$

It appears that the components of $\mathbf{S^{II}}$ are identical or have opposite sign as those of $\mathbf{S^{I}}$. As a consequence, the plane components of $[\boldsymbol{\varepsilon}^\star]$ (Equation 5) reduce to

$$\begin{aligned} [\varepsilon_1^\star] &= -2s_{14}^*\Sigma_4 - 2s_{16}^*\Sigma_6 + [\varepsilon_1^p] \\ [\varepsilon_3^\star] &= -2s_{34}^*\Sigma_4 - 2s_{36}^*\Sigma_6 + [\varepsilon_3^p] \\ [\varepsilon_5^\star] &= -2s_{45}^*\Sigma_4 - 2s_{56}^*\Sigma_6 + [\varepsilon_5^p] \end{aligned} \tag{10}$$

Hence, out of the 6 components of $\mathbf{\Sigma}$ expressed in the twin boundary frame, only Σ_4 and Σ_6 act upon the general incompatibility stress tensor $\boldsymbol{\sigma}^{\boldsymbol{inc\star}}$. Σ_6 corresponds directly to the macroscopic resolved shear stress on the twinning system. Σ_4 is the other anti-plane shear stress component. It acts also on the $\mathbf{K_1}$ plane, but in a direction orthogonal to $\boldsymbol{\eta_1}$. As a consequence, for uniaxial loading, incompatibility stresses due to elastic mismatch around general type I twin boundaries may be insignificant if the $\mathbf{K_1}$ planes are oriented nearly parallel or perpendicular to the loading axis. On the other hand, incompatibility stresses may be enhanced if $\mathbf{K_1}$ planes get close to a 45 ° orientation from the loading axis. Note also that concerning the tensor $\mathbf{G}$ (Equation 7), the simplification due to type I twin configuration leads to $G_{PP'}(\tilde{s}) = G_{PP'}(s^*)$ since $\tilde{s}_{ij} = f^{II}s_{ij}^* + f^I s_{ij}^*$ for $i, j = 1, 3, 5$. It means that for type I twins, volume fractions have no influence on the orientation of the incompatibility stress tensor. They act only upon the incompatibility stress magnitudes.

4.2. *Type II twins*

For type II twinning, the orientation of the twin lattice relative to the parent one corresponds to a 180 ° rotation around $\boldsymbol{\eta_1}$ [31]. Hence, $\mathbf{S^{II}}$ is deduced from $\mathbf{S^{I}}$ by a 180 ° rotation around $\mathbf{e_1^*}$

$$\mathbf{S^{II}} = \begin{bmatrix} s_{11}^* & s_{12}^* & s_{13}^* & s_{14}^* & -s_{15}^* & -s_{16}^* \\ s_{12}^* & s_{22}^* & s_{23}^* & s_{24}^* & -s_{25}^* & -s_{26}^* \\ s_{13}^* & s_{23}^* & s_{33}^* & s_{34}^* & -s_{35}^* & -s_{36}^* \\ s_{14}^* & s_{24}^* & s_{34}^* & s_{44}^* & -s_{45}^* & s_{46}^* \\ -s_{15}^* & -s_{25}^* & -s_{35}^* & -s_{45}^* & s_{55}^* & s_{56}^* \\ -s_{16}^* & -s_{26}^* & -s_{36}^* & s_{46}^* & s_{56}^* & s_{66}^* \end{bmatrix} \tag{11}$$

Again, the components of $\mathbf{S^{II}}$ are identical or have opposite sign as those of $\mathbf{S^{I}}$. However, unlike the case of the type I twin, the 6 components of $\mathbf{\Sigma}$ act now upon the incompatibility stress tensor, as it is shown from the plane components of $[\boldsymbol{\varepsilon}^\star]$

$$
\begin{aligned}
[\varepsilon_1^\star] &= -2s_{15}^*\Sigma_5 - 2s_{16}^*\Sigma_6 + [\varepsilon_1^p] \\
[\varepsilon_3^\star] &= -2s_{35}^*\Sigma_5 - 2s_{36}^*\Sigma_6 + [\varepsilon_3^p] \\
[\varepsilon_5^\star] &= -2s_{15}^*\Sigma_1 - 2s_{25}^*\Sigma_2 - 2s_{35}^*\Sigma_3 - 2s_{45}^*\Sigma_4 + [\varepsilon_5^p]
\end{aligned}
\tag{12}
$$

5. $\Sigma 3 < 111 >$ twin boundary

In this subsection, it is considered that the planar interfaces of Figure 1 are $\Sigma 3 < 111 >$ twin boundaries which are the twin boundaries mostly encountered in f.c.c. metals [31]. These twin boundaries satisfy relations of symmetry for both type I and type II twins. The $\mathbf{K_1}$ plane corresponds to a (111) crystallographic plane, whereas $\boldsymbol{\eta_1}(\equiv \mathbf{e_1^*})$ corresponds to a $< 11\overline{2} >$ crystallographic direction. In the single crystal frame, the elastic compliances tensor associated to a cubic lattice writes

$$
\mathbf{S} = \begin{bmatrix}
s_{11} & s_{12} & s_{12} & 0 & 0 & 0 \\
s_{12} & s_{11} & s_{12} & 0 & 0 & 0 \\
s_{12} & s_{12} & s_{11} & 0 & 0 & 0 \\
0 & 0 & 0 & s_{44} & 0 & 0 \\
0 & 0 & 0 & 0 & s_{44} & 0 \\
0 & 0 & 0 & 0 & 0 & s_{44}
\end{bmatrix}
\tag{13}
$$

The elastic compliances tensor of crystal I in the twin boundary frame can then be deduced from the rotation that transforms the vectors $\frac{1}{\sqrt{6}}[11\overline{2}]$ and $\frac{1}{\sqrt{3}}[111]$ into [100] and [010], respectively. As a result, the expression of $\mathbf{S^I}$ in the twin boundary frame is

$$
\mathbf{S^I} = \begin{bmatrix}
s_{11}^* & s_{12}^* & s_{13}^* & 0 & 0 & s_{16}^* \\
s_{12}^* & s_{22}^* & s_{12}^* & 0 & 0 & 0 \\
s_{13}^* & s_{12}^* & s_{11}^* & 0 & 0 & -s_{16}^* \\
0 & 0 & 0 & s_{44}^* & -2s_{16}^* & 0 \\
0 & 0 & 0 & -2s_{16}^* & -2(s_{13}^* - s_{11}^*) & 0 \\
s_{16}^* & 0 & -s_{16}^* & 0 & 0 & s_{44}^*
\end{bmatrix}
\tag{14}
$$

where s_{ij}^* are related to the 3 independent elastic compliances s_{11}, s_{12}, and s_{44} as follows

$$
\begin{aligned}
s_{11}^* &= \tfrac{1}{4}\left(2s_{11} + 2s_{12} + s_{44}\right) \quad , s_{16}^* = \tfrac{\sqrt{2}}{6}\left(-2s_{11} + 2s_{12} + s_{44}\right) \\
s_{12}^* &= \tfrac{1}{6}\left(2s_{11} + 4s_{12} - s_{44}\right) \quad , s_{22}^* = \tfrac{1}{3}\left(s_{11} + 2s_{12} + s_{44}\right) \\
s_{13}^* &= \tfrac{1}{12}\left(2s_{11} + 10s_{12} - s_{44}\right) , s_{44}^* = \tfrac{1}{3}\left(4s_{11} - 4s_{12} + s_{44}\right)
\end{aligned}
\tag{15}
$$

5.1. *Incompatibility stresses*

Combining Equations 6, 7, 9 (or 11), 10 (or 12) and 14 , the expression of the incompatibility stress tensor simplifies tremendously for a $\Sigma 3 < 111 >$ boundary. In the twin boundary frame, the plane components of $\boldsymbol{\sigma}^{\boldsymbol{inc\star}}$ are

$$\begin{aligned}
\sigma_1^{inc\star} &= \frac{-2s_{16}^*}{s_{13}^* - s_{11}^*}\Sigma_6 + \frac{s_{11}^*\left[\varepsilon_1^p\right] - s_{13}^*\left[\varepsilon_3^p\right]}{s_{13}^{*2} - s_{11}^{*2}} \\
\sigma_3^{inc\star} &= \frac{2s_{16}^*}{s_{13}^* - s_{11}^*}\Sigma_6 + \frac{s_{11}^*\left[\varepsilon_3^p\right] - s_{13}^*\left[\varepsilon_1^p\right]}{s_{13}^{*2} - s_{11}^{*2}} \\
\sigma_5^{inc\star} &= \frac{2s_{16}^*}{s_{13}^* - s_{11}^*}\Sigma_4 + \frac{\left[\varepsilon_5^p\right]}{2\left(s_{13}^* - s_{11}^*\right)}
\end{aligned} \tag{16}$$

Concerning the contribution arising from the difference of plastic strains, it can be noticed the symmetry between the components 1 and 3 and the exclusive dependence between the shear stress and the plastic shear strain component. Concerning the contribution arising from the macroscopic stress tensor, the presence of a common pre-factor should be underlined. Substituting the elastic compliances of the crystal frame thanks to Equation 15 and introducing the elastic anisotropy factor A, the expression of $\boldsymbol{\sigma}^{\mathbf{inc}\star}$ can be even more simplified. In the case of pure elasticity, its expression in the twin boundary frame is

$$\boldsymbol{\sigma}^{\mathbf{inc}\star} = 2\sqrt{2}\frac{A-1}{A+2}\begin{bmatrix} -\Sigma_6 & 0 & \Sigma_4 \\ 0 & 0 & 0 \\ \Sigma_4 & 0 & \Sigma_6 \end{bmatrix} \tag{17}$$

The above stress tensor is purely deviatoric. Its principal stresses are $2\sqrt{2}\frac{A-1}{A+2}(0, T, -T)$ with $T = \sqrt{\Sigma_4^2 + \Sigma_6^2}$. T is the tangential component of the macroscopic traction vector acting on the twin plane. Hence, $\boldsymbol{\sigma}^{\mathbf{inc}\star}$ just corresponds to a shear stress state in the frame deduced from the principal frame by a 45° or a -45° rotation around the first principal direction ($\equiv \mathbf{e_2^*}$). Considering the frame deduced by a -45° rotation, the basis vectors have the following expressions in the twin boundary frame

$$\mathbf{U_1} = \begin{bmatrix} 0 \\ 1 \\ 0 \end{bmatrix}, \mathbf{U_2} = \begin{bmatrix} \frac{\sqrt{T-\Sigma_6}+\sqrt{T+\Sigma_6}}{2\sqrt{T}} \\ 0 \\ \frac{\sqrt{T+\Sigma_6}-\sqrt{T-\Sigma_6}}{2\sqrt{T}} \end{bmatrix}, \mathbf{U_3} = \begin{bmatrix} \frac{\sqrt{T-\Sigma_6}-\sqrt{T+\Sigma_6}}{2\sqrt{T}} \\ 0 \\ \frac{\sqrt{T+\Sigma_6}+\sqrt{T-\Sigma_6}}{2\sqrt{T}} \end{bmatrix} \tag{18}$$

Consequently, in the frame $(\mathbf{U_1}, \mathbf{U_2}, \mathbf{U_3})$, the incompatibility stress tensors in the parent (I) and in the twin (II) can be written as

$$\boldsymbol{\sigma}^{\mathbf{incI,II}} = \begin{bmatrix} 0 & 0 & 0 \\ 0 & 0 & \tau^{I,II} \\ 0 & \tau^{I,II} & 0 \end{bmatrix} \text{ with } \begin{cases} \tau^I = -2\sqrt{2}\frac{A-1}{A+2}Tf^{II} \\ \tau^{II} = 2\sqrt{2}\frac{A-1}{A+2}Tf^I \end{cases} \tag{19}$$

The additional shear stresses in the twin and in the parent both act on a same plane that is orthogonal to twin plane and along opposite directions that are parallel to twin plane. Their relative magnitude is the inverse of the volume fraction ratio. The specific direction of these shears solely depends on T and on the macroscopic resolved shear on the twinning system. As mentioned in the Introduction, the remarkable simplicity of this scalar result was first found, in case of equal volume fraction, by Neumann [13], who was interested in fatigue crack initiation. Since

cracks occurs preferentially at free surfaces, Neumann used this bulk result to estimate incompatibility surface stresses at twin boundaries thanks to an approximate and simplified treatment [3, 4, 13].

5.2. *Resolved shear stresses on slip systems considering pure elasticity*

In this subsection, the expressions of the resolved shear stresses (RSSs) on the classical 12 f.c.c. slip systems (s) for perfect dislocations in the parent and in the twin are looked after in the case of pure elasticity. They are computed from Equation 6 as

$$\tau^s_{parent} = \mathbf{R^s_{parent}} : \left(\boldsymbol{\Sigma} - f_{twin}\boldsymbol{\sigma}^{\mathbf{inc\star}}\right) \ , \ \tau^s_{twin} = \mathbf{R^s_{twin}} : \left(\boldsymbol{\Sigma} + (1-f_{twin})\,\boldsymbol{\sigma}^{\mathbf{inc\star}}\right) \tag{20}$$

where $\mathbf{R}^s_{parent/twin}$ are the Schmid orientation tensors and f_{twin} is the twin volume fraction ($f_{twin} = f^{II}$). The case of a uniaxial loading of magnitude Σ_u is further considered. Then, ϕ the angle between $\mathbf{n^{K_1}}$ and the loading axis ($0 \leq \phi \leq 90^\circ$) and ψ, a rotation angle around $\mathbf{n^{K_1}}$ ($0 \leq \psi \leq 360^\circ$), are introduced (see Figure 2). In our configuration, the $\mathbf{K_1}$ plane is a B plane of the Schmid and Boas' notation [32] (see the notations in Table 1). In the loading frame, $\mathbf{n^{K_1}} = [\cos\phi, 0, \sin\phi]$ whereas $\psi = 0$ corresponds to $\boldsymbol{\eta_1} = [\sin\phi, 0, -\cos\phi]$. Using the expression in pure elasticity of $\boldsymbol{\sigma}^{\mathbf{inc\star}}$ given by Equations 17 or 19, the computation of the above RSSs can be performed analytically. As a result, the RSSs on slip systems (s) read

$$\begin{aligned} \tau^s_{parent} &= \tau^s_{appl(parent)} - \frac{8\sqrt{3}}{9} f_{twin} \frac{A-1}{A+2} \chi^s_{parent} T \\ \tau^s_{twin} &= \tau^s_{appl(twin)} + \frac{8\sqrt{3}}{9} (1-f_{twin}) \frac{A-1}{A+2} \chi^s_{twin} T \end{aligned} \tag{21}$$

Notation	A2	A3	A6	B2	B4	B5	C1	C3	C5	D1	D4	D6
Slip planes	$(\bar{1}11)$	$(\bar{1}11)$	$(\bar{1}11)$	(111)	(111)	(111)	$(\bar{1}\bar{1}1)$	$(\bar{1}\bar{1}1)$	$(\bar{1}\bar{1}1)$	$(1\bar{1}1)$	$(1\bar{1}1)$	$(1\bar{1}1)$
Slip directions	$[0\bar{1}1]$	$[101]$	$[110]$	$[0\bar{1}1]$	$[\bar{1}01]$	$[\bar{1}10]$	$[011]$	$[101]$	$[\bar{1}10]$	$[011]$	$[\bar{1}01]$	$[110]$

Table 1. Schmid and Boas' notations for slip systems in f.c.c. crystals.

where $\tau^s_{appl(parent/twin)} = \mathbf{R^s_{parent/twin}} : \boldsymbol{\Sigma}$ and $T = (\cos\phi \sin\phi)\,\Sigma_u$. The functions $\chi^s_{parent/twin}$ depend only on ψ and write with the Schmid and Boas convention as

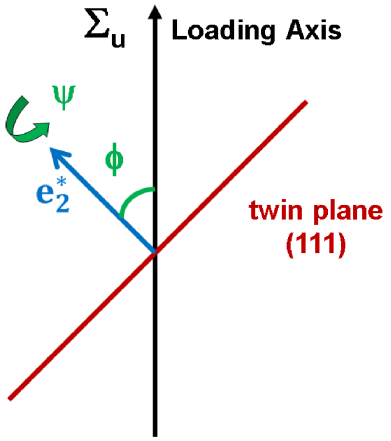

Figure 2. Uniaxial loading test where the normal to the twin boundary plane ($\mathbf{n^{K_1}} \equiv \mathbf{e_2^*}$) makes an angle ϕ with the loading axis. ψ is a rotation angle around $\mathbf{n^{K_1}}$.

$$
\begin{array}{ll}
\chi^{A2}_{parent} = \sqrt{3}\cos\left(\psi - \frac{5\pi}{6}\right) & , \chi^{A2}_{twin} = \sqrt{3}\cos\left(\psi + \frac{\pi}{2}\right) \\
\chi^{A3}_{parent} = \cos\left(\psi + \pi\right) & , \chi^{A3}_{twin} = \cos\left(\psi + \frac{\pi}{3}\right) \\
\chi^{A6}_{parent} = \cos\left(\psi + \frac{\pi}{3}\right) & , \chi^{A6}_{twin} = \cos\left(\psi - \frac{\pi}{3}\right) \\
\chi^{B2}_{parent} = 0 & , \chi^{B2}_{twin} = 0 \\
\chi^{B4}_{parent} = 0 \ , & , \chi^{B4}_{twin} = 0 \\
\chi^{B5}_{parent} = 0 & , \chi^{B5}_{twin} = 0 \\
\chi^{C1}_{parent} = \cos\left(\psi - \frac{2\pi}{3}\right) & , \chi^{C1}_{twin} = \cos\left(\psi + \frac{2\pi}{3}\right) \\
\chi^{C3}_{parent} = \cos\left(\psi + \frac{2\pi}{3}\right) & , \chi^{C3}_{twin} = \cos\left(\psi\right) \\
\chi^{C5}_{parent} = \sqrt{3}\cos\left(\psi - \frac{\pi}{2}\right) & , \chi^{C5}_{twin} = \sqrt{3}\cos\left(\psi + \frac{5\pi}{6}\right) \\
\chi^{D1}_{parent} = \cos\left(\psi + \pi\right) & , \chi^{D1}_{twin} = \cos\left(\psi + \frac{\pi}{3}\right) \\
\chi^{D4}_{parent} = \sqrt{3}\cos\left(\psi + \frac{5\pi}{6}\right) & , \chi^{D4}_{twin} = \sqrt{3}\cos\left(\psi + \frac{\pi}{6}\right) \\
\chi^{D6}_{parent} = \cos\left(\psi - \frac{\pi}{3}\right) & , \chi^{D6}_{twin} = \cos\left(\psi + \pi\right)
\end{array}
\tag{22}
$$

The occurrence of a 60 ° period due to the f.c.c. symmetry should be underlined. As a matter of fact, when ψ is rotated by 60 °, only the naming of slip systems is modified, the list of the absolute $\chi^s_{parent/twin}$ values remains actually unchanged. Very interestingly, roundups of slip systems can also be deduced from the expressions of $\chi^s_{parent/twin}$:

(i) systems $B2$, $B4$ and $B5$ for which $\chi^s_{parent/twin} = 0$ since their slip plane is common to twin plane (cf. Equation 8),

(ii) systems $A2$, $C5$ and $D4$ for which $\chi^s_{parent/twin}$ writes as $\sqrt{3}$ times a cosine function of ψ,

(iii) systems $A3$, $A6$, $C1$, $C3$, $D1$, $D6$ for which $\chi^s_{parent/twin}$ just writes as a cosine function of ψ.

Considering situations with single slip in the parent and single slip in the twin, the first two groups of slip systems could be retrieved by looking for the active systems that fulfil a zero plastic incompatibility condition, i.e. $\left[\varepsilon^p_P\right] = 0$ (cf. Equations 2-7). Such a condition is actually equivalent to the fulfilment of the tangential

continuity of the plastic distortion (see the proof in [14]) which corresponds to the conservation of the Burgers vector in case of dislocation glide only (no boundary motion). It was examined in [33] for a general single slip/single slip configuration at a planar interface. It was shown that it is satisfied either when both slip planes are common with the interface plane, or for a same plastic slip on both sides with slip planes in a 'mirror configuration' and common slip directions belonging to the interface plane. The first situation is precisely met by systems $B2$, $B3$ and $B4$ where slip can develop freely without inducing any plastic incompatibility.

The second situation is met by pairs of systems $A2^{parent}/D4^{twin}$, $C5^{parent}/A2^{twin}$ and $D4^{parent}/C5^{twin}$. Such pair of systems allow cross-slip of perfect screw dislocations at the twin boundary [34, 35]. They were recently highlighted in microcompression experiments on copper bicrystals with $\Sigma 3 < 111 >$ twin boundaries (see the figure 3 in [36]). These pairs of systems can also be called pairs of compatible systems, in the sense that, for a same slip in both systems, no supplementary incompatibility stress will be generated. This assertion is in perfect agreement with the experimental evidence of [36] which showed no strengthening and no strain-hardening effect associated to the presence of the twin boundary. Actually, slip on these systems will also induce no supplementary lattice misorientation whereas the misorientation due to elastic incompatibilities alone is very negligible [14]. This case corresponds practically to 'degenerate interfaces' according to the terminology used by Ortiz and Repetto, who were interested in dislocation structures formation in single crystals thanks to global compatibility conditions in the absence of long-range stress [37]. Ortiz and Repetto considered, however, the presence of a misorientation between the two variants since the misorientation is precisely related to the dislocation content at the interface [14, 37].

The expressions in Equation 22 show that incompatibility resolved shear stresses on couple of slip systems that allow cross-slip of perfect screw dislocations are those that will increase the most with the loading stress. Hence, it is interesting to underline that cross-slip may be promoted at the twin boundary compared to other mechanisms thanks to elastic anisotropy and induced incompatibility stresses. However, for a complete analysis of possible promotion of crossing mechanisms at the twin boundary by modification of local stresses, one should also consider the numerous mechanisms that imply partial dislocations, as detailed in [34, 35, 38].

6. Numerical applications for lamellar $\Sigma 3 < 111 >$ twin structures

As mentioned in the Introduction, TWIP steels are promising materials due to their enhanced mechanical properties. It is generally admitted that the activation of twinning is sequential: a primary twinning system is first activated before the activation of a secondary system takes place at larger strains [18]. For a Fe-22Mn-0.6C wt.% TWIP steel, Allain [18] observed that the proportion of grains with a single twinning system increased until 50% at 15% of uniaxial strain, then decreased and stabilized above 20% until the end of the test. For a similar steel at 30% and 40% of uniaxial strain, Gutierrez-Urrutia and Raabe [19] pointed out that 30% of the grains fell in the case of single lamellar twin structure whereas 60% of the grains were concerned with two active twinning systems. Accordingly, the present numerical analysis will only focus on the case of a lamellar $\Sigma 3 < 111 >$ twin structure [31] along a unique primary system, for which the approximation of a periodic layered structure is directly relevant. Hence, good estimates of the incompatibility stress field in the elastic regime are expected from Equations 17 or 19. The case of a uniaxial loading of magnitude Σ_u is still considered. The RSSs on the different slip systems can thus be directly estimated from Equations 21 and

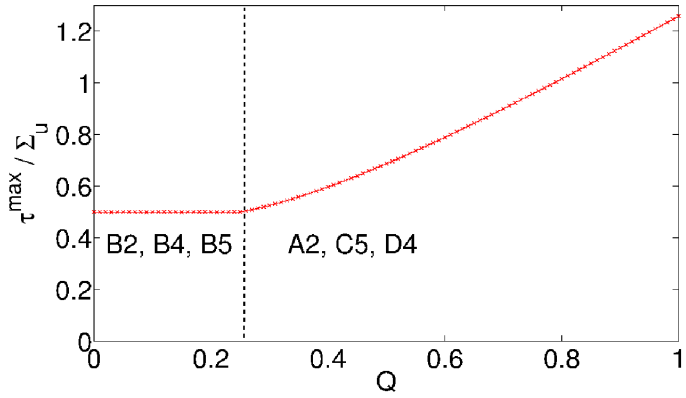

Figure 3. Variation with Q of the maximal RSS in the parent or in the twin among all the possible orientations of the twin boundaries.

22. The RSSs depend on the value of Σ_u, on the crystallographic orientation of the twin boundaries which is given by the angles (ϕ, ψ), on the twin volume fraction f_{twin} and on the elastic anisotropy factor A.

Moreover, in order to make easier the forthcoming analyses, the parameter Q is introduced as $Q_{parent} = f_{twin}\frac{A-1}{A+2}$ and $Q_{twin} = (1 - f_{twin})\frac{A-1}{A+2}$. Hence, for a given orientation of the twin boundaries, the RSS values are bijective functions of Q whereas a given RSS value can correspond to an infinite number of twin volume fraction and elastic anisotropy factor combinations (cf. Equation 21). The classical Schmid hypothesis (absence of incompatibility stresses) is retrieved with $Q = 0$, which can correspond either to the elastic isotropic case ($A = 1$) or to the single phase case ($f_{twin} = 0$ or 1). The value of Q in one phase varies linearly with the volume fraction of the other phase. Hence, for values of elastic anisotropy factor close to those of copper or austenitic steels ($A = 3 - 4$), the range of Q is between 0 and $0.4 - 0.5$.

6.1. *Maximal resolved shear stress*

In the first place, let us consider the maximal RSS in absolute value, τ^{max}, that can be reached in the twin or in the parent among all the possible orientations of the twin boundaries. Figure 3 shows the variation of τ^{max} with Q ($Q = Q_{parent}$ if τ^{max} is in the parent and $Q = Q_{twin}$ if τ^{max} is in the twin). It is seen that for low values of Q ($Q < 0.25$), τ^{max} is only found on slip systems $B2$, $B4$ or $B5$ with a value of $0.5\Sigma_u$. As explained above, the resolved incompatibility stresses are zero on these systems which are parallel to twin plane. It is thus expected to retrieve the classical maximal Schmid factor value of 0.5. However, for the other systems, Figure 3 indicates that τ^{max} is always lower than $0.5\Sigma_u$ for $Q < 0.25$, meaning that elastic incompatibilities reduce the RSSs for the 'normally best oriented' systems. Therefore, the presence of twins does not necessarily favour the early development of slip. It should be noticed also that, when the maximal RSS is on the twin plane in the parent and in the twin, it acts forcedly along the same slip direction since the twin plane is an invariant plane and $\sigma_A^{inc\star} = 0$ (cf. Equation 8).

For $Q > 0.25$, the situation changes. τ^{max} is now only found on systems $A2$, $C5$ and $D4$ which are the other systems which may allow the development of compatible plastic distortion. For $Q > 0.25$, τ^{max} increases linearly with Q. It can reach the considerable value of $1.26\Sigma_u$ for the maximal theoretical value of Q ($Q = 1$ for $f_{twin} = 0$ or 1 and $A \to \infty$). Accordingly, elastic incompatibilities at

twin boundaries can widen tremendously the range of RSS values in comparison to the restricted range of $0-0.5\Sigma_u$ for a grain without twins. The significant influence of the twin volume fraction on this result should be underlined. Indeed, in case of equal volume fraction of twin and parent phases, the maximal value of Q is 0.5 and τ^{max} is then limited by a maximal value of $0.69\Sigma_u$ (Figure 3).

6.2. *Single slip promotion*

In this subsection, the ratio R, in a given phase (twin or parent), between the highest RSS and the second highest RSS in absolute value is considered in order to highlight potential single slip situations. In uniaxial testing of single crystals, the values of R are very close to 1 for multiple or double slip oriented crystals whereas single slip oriented crystals have high values of R. A well-known orientation for single slip is $< 123 >$ [39] and corresponds to $R = 1.33$. Actually, the highest value of R within the standard stereographic triangle is found for a loading along a $< 13\ 21\ 34 >$ direction [40]. Such an orientation yields $R = 1.38$.

Figure 4 shows the evolution of the maximal value of R in the parent or in the twin among all the possible orientations of the twin boundaries as a function of Q. As previously explained, the case $Q = 0$ is actually similar to a single crystal testing and thus the value $R^{max} = 1.38$ is retrieved. In this case, the highest RSS corresponding to R^{max} can belong to any system. However, as soon as $Q > 0$, the value of R^{max} increases and the highest RSS corresponding to R^{max} is only found on the preferential set of slip systems $B2$, $B4$, $B5$. There is a switch of this preferential set at $Q = 0.42$ for systems $A3$, $A6$, $C1$, $C3$, $D1$ and $D6$. For $0 < Q < 0.42$, the highest RSSs thus remain unchanged at $0.5\Sigma_u$ while the incompatibility stresses can lower or increase the RSSs on the other systems. Firstly, the lowering effects on the second highest RSSs are predominant and R^{max} increases. It reaches a maxima at $Q = 0.31$ corresponding to $R^{max} = 1.80$. Then, the increasing effects take over, meaning that the second highest RSSs find now themselves on systems of which the RSSs increase with Q. As a consequence, R^{max} decreases until the highest RSSs leave the B planes at $Q = 0.42$. After that, R^{max} increases linearly since the highest RSSs are now those that increase the most. The saturation value of $R^{max} = 2$ is finally reached at $Q = 0.83$. This saturation value is the maximal theoretical value of R that it is possible to get for a f.c.c. symmetry considering any possible stress field. This theoretical maxima actually corresponds to the case of a pure shear applied to a single crystal when the RSS on a slip system matches exactly the macroscopic shear stress (the second highest RSS is on a system on the same plane with slip direction at 60° and thus, is half the value of the macroscopic shear stress).

Figure 5 shows the variations of all the RSSs, in the parent and in the twin phases, for the typical situation of twin boundaries tilted at 45° from the loading axis. The cases $Q_{parent} = 0$ or $Q_{twin} = 0$ (Figures 5a and b) show that the highest RSSs are not always on B planes according to the values of ψ and, if this is the case, are not much higher than the highest RSSs on the other planes. For $Q_{parent} = 0.2$ or $Q_{twin} = 0.2$ (Figures 5c and d), it is seen that the highest RSSs on planes other than B planes have decreased considerably due to incompatibility stresses. As a consequence, the highest RSSs are now, always on B planes and with much higher values than RSSs on the other planes. Accordingly, planar slip parallel to twin plane is strongly promoted and the probability of single slip is also very high. For higher values of Q (Figure 5f with $Q_{twin} = 0.6$), the highest RSSs are no more on B planes but on systems $A2$, $C5$ and $D4$. In this case, the probability of single slip is low. Figure 6a gives actually the corresponding variations of R with ψ in the

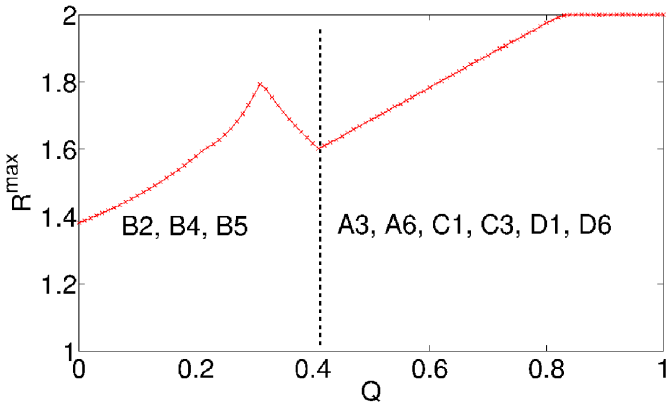

Figure 4. Variation with Q of the maximal value of the ratio R in the parent or in the twin among all the possible orientations of the twin boundaries.

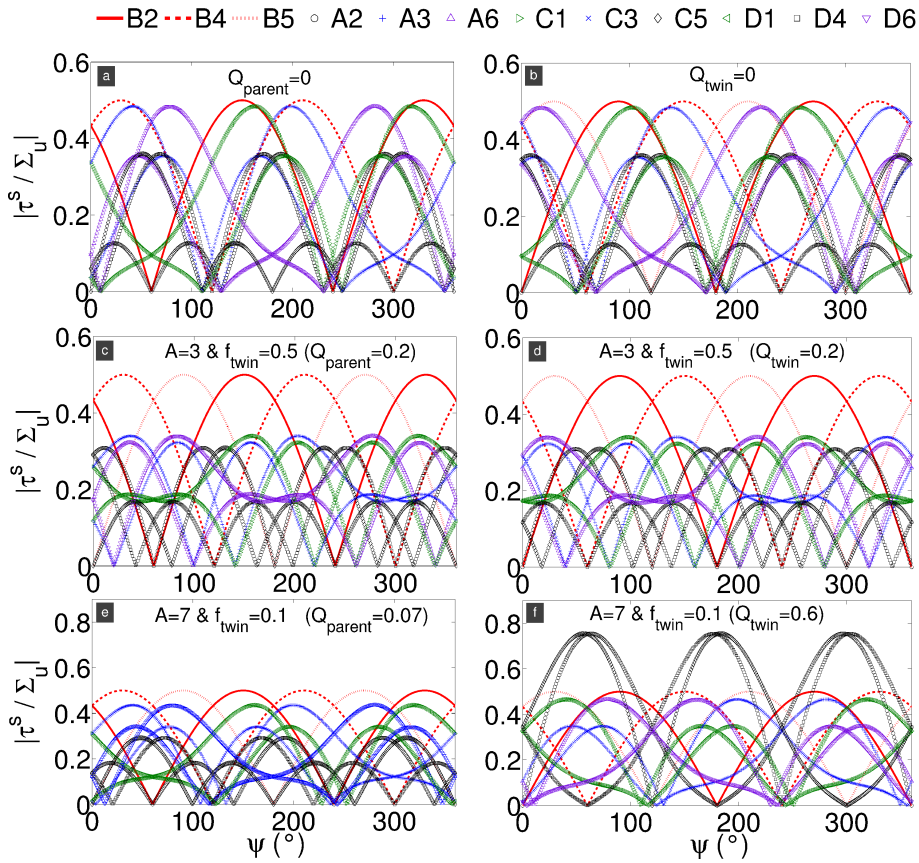

Figure 5. Variation with ψ of the RSSs in the parent (left: a, c, e) and in the twin (right: b, d, f) for $\phi = 45^\circ$ and different values of Q.

parent. For $Q_{parent} = 0$, R goes as thin periodic peaks reaching maximal values just above 1.2. It thus remains quite low in most of the range of the ψ values. An almost similar situation is met for $Q = 0.6$. On the contrary, for $Q_{parent} = 0.2$, R is above 1.4 in a wide range of the ψ values. Figure 6b provides a similar analysis for $\phi = 20^\circ$ and shows that the picture is completely different. Single slip situations can occur in the case $Q_{parent} = 0$, with peak values of R close to the theoretical single crystal maximal value of 1.38, whereas a strong promotion of double slip is observed at $Q_{parent} = 0.2$ since R remains always lower than 1.05.

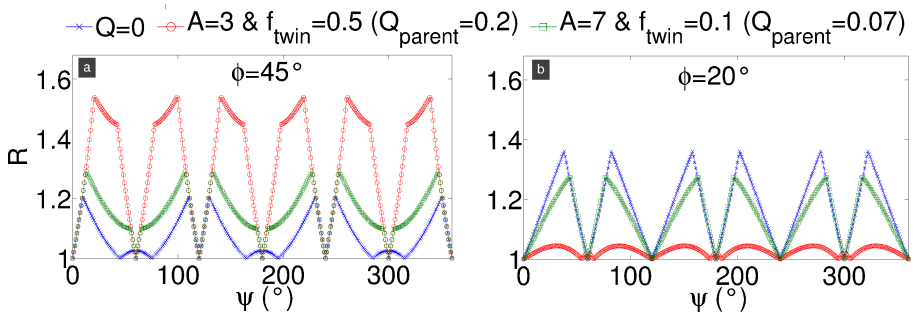

Figure 6. Variation with ψ of the ratio R in the parent for $\phi = 45^\circ$ and $\phi = 20^\circ$ and different values of Q.

Promotion of single slip on planes parallel to twin plane in both, the parent and the twin phases, is particularly interesting since then, slip occurs on the same system in the whole grain and dislocation motion is not constrained by twin boundaries. Such a situation is displayed in Figures 5c and d for $\phi = 45^\circ$ and $Q_{parent} = Q_{twin} = 0.2$, i.e. for the same volume fraction of twin and parent phases. The question is then to know if similar situations can be retrieved for other conditions of twin boundary orientation, elastic anisotropy factor and twin volume fraction. Figure 7 provides therefore a frequency map of the occurrence of situations of single slip parallel to twin plane in function of A and f_{twin}. For relevancy, frequencies are only computed out of orientations favourable for twin activation. In TWIP steels, a simple Schmid analysis is not sufficient to explain the occurrence of twinning but there is yet a general trend that twinning correlates more or less with high Schmid factor values, at least at the beginning of the deformation [19, 20, 41, 42]. In particular, orientations generally considered to be favourable for twin activation are those that display higher maximal Schmid factor value for twinning than for slip [41, 42]. Hence, in our computation, only twin boundary orientations of which the Schmid factor is maximal among the 12 $(111)[11\bar{2}]$ twinning systems and greater than the maximal absolute Schmid factor of the 12 $(111)[\bar{1}01]$ slip systems are taken into account. Those situations correspond to $28.1^\circ \leq \phi \leq 77.9^\circ$ whilst ψ can vary from 0° to no less than -25.7°. Then, among these orientations, Figure 7 displays the percentage of orientations characterized by $R > 1.2$ and maximal RSS on the slip plane parallel to twin plane, simultaneously in the parent and in the twin. Figure 7 shows a large area with frequencies higher than 20% or 25%. For comparison, the same computation based on the classical Schmid law (i.e., without consideration of incompatibility stresses) would have yield a 0% frequency.

Similarly, Figure 8 displays only the frequency map of simultaneous slip parallel to twin plane, i.e., the percentage of orientations characterized maximal RSS on the slip plane parallel to twin plane in the parent and in the twin. In this case, frequencies greater than 70% are reached whereas the same computation based on the Schmid law gives 17%.

Finally, Figure 9 displays the frequency map of single slip parallel to twin plane in the parent phase only, i.e., the percentage of orientations characterized, in the parent phase, by $R > 1.2$ and maximal RSS on the slip plane parallel to twin plane. In this case, the frequency can be plotted directly in function of Q_{parent} since RSSs values in the parent are bijective functions of Q_{parent}. The initial frequency at $Q_{parent} = 0$ (i.e., without twins) is 16%. Then, it increases until $Q_{parent} = 0.18$ where a maximum is reached ($\sim$ 29%). It is interesting to note that, the same maximal frequency is obtained in Figure 7 when single slip conditions parallel to twin plane are applied in both phases. Afterwards, the frequency decreases, becomes less than 16% for $Q_{parent} > 0.31$ and finally zero for $Q_{parent} > 0.40$. It

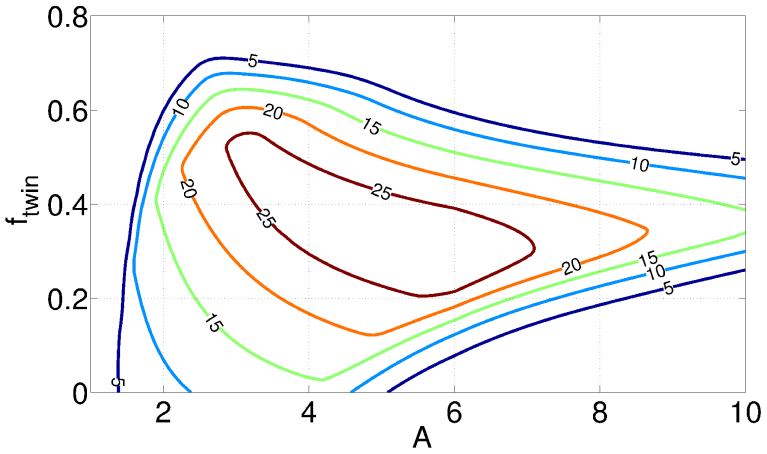

Figure 7. Frequency map of simultaneous single slip parallel to twin plane in function of A and f_{twin}. Values are given in % and correspond to twin boundary orientation frequencies when, in the parent and in the twin, $R > 1.2$ and maximal RSS is on the slip plane parallel to twin plane. Only orientations favourable to the twin activation are considered in the computation (see text). The same computation based on the Schmid law gives 0%.

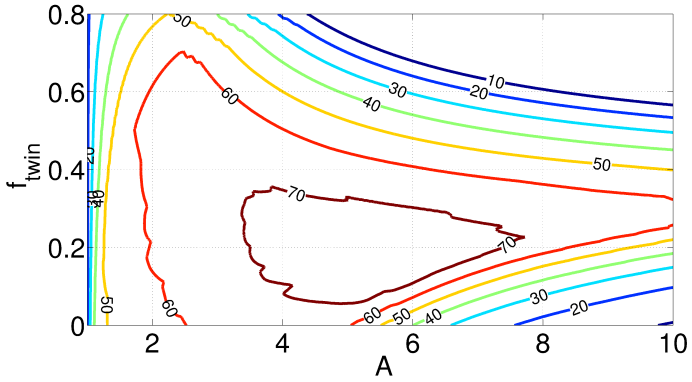

Figure 8. Frequency map of simultaneous slip parallel to twin plane in function of A and f_{twin}. Values are given in % and correspond to twin boundary orientation frequencies when, in the parent and in the twin, maximal RSS is on the slip plane parallel to twin plane. Only orientations favourable to the twin activation are considered in the computation (see text). The same computation based on the Schmid law gives 17%.

is noteworthy that real situations almost always correspond to the case $Q < 0.31$. For instance, extreme values like $f_{twin} = 0.5$ and $A = 8$ yield $Q_{parent} = 0.35$.

7. Discussion

For lamellar $\Sigma 3 < 111 >$ twin structures, results show that planar slip parallel to twin plane is greatly promoted when the tilt between the twin plane and the loading axis get close to 45°. More generally, it appears that the combined effect of elastic anisotropy and presence of twin boundaries promotes very strongly simultaneous slip parallel to twin plane in the parent and in the twin. It also clearly enhances the possibility of single slip in this plane. These promotions occur in relatively large physical domains which depend on the twin volume fraction, the elastic anisotropy factor and the twin boundary orientation. In the present analysis, only orientations favourable for twin activation were considered in order to be as realistic as possible. Figure 7 indicates that simultaneous promotion of single slip parallel to twin plane occurs roughly for $A = 3 - 6$ and $f_{twin} = 0.2 - 0.4$. For simultaneous pro-

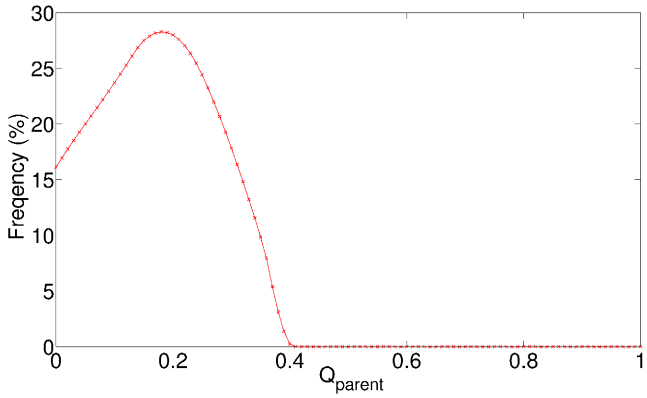

Figure 9. Frequency of single slip parallel to twin plane in the parent phase in function of Q_{parent}. Values are given in % and correspond to twin boundary orientation frequencies when, in the parent, $R > 1.2$ and the maximal RSS is on on the slip plane parallel to twin plane. Only orientations favourable to the twin activation are considered in the computation (see text).

motion of slip parallel to twin plane only, the domain is larger with $A = 2 - 7$ and $f_{twin} = 0 - 0.5$. These values are pretty much realistic considering the literature data on TWIP steels [19, 20, 43, 44]. It must be noticed however, that for single slip promotion, values of twin volume fraction above 0.2 can be reached in grains with single lamellar twin structure but only late in the deformation process, when many other grains already display two twin planes. For instance, for a Fe-22Mn-0.6C wt.% TWIP steel, Gutierrez-Urrutia and Raabe [19] measured an average twin spacing around 300 nm and an average twin thickness ranging from 30 to 100 nm, which leads to twin volume fractions in grains between 0.17 and 0.40 according to the stereological relation of Fullman [45] ($f_{twin} = \frac{2e}{2e+t}$ with e the mean twin thickness and t the mean twin spacing). Furthermore, the elastic anisotropy of TWIP steels is often assumed to be close to that of other similar austenitic steels ($A \sim 3.3 - 3.9$). There is, however, a lack of experimental measurements of single crystal elastic constants in the literature. A very recent experimental study by nanoindentation yielded $A = 2.11/2.22$ for two Fe-(22/25)Mn-3Al-3Si wt.% alloys [43]. The authors of this study [43] underlined, nevertheless, that for TWIP steels in the antiferromagnetic regime, such as Fe-22Mn-0.6C wt.% and Fe-28Mn-3Al-3Si wt.%, the value of A is expected to be much higher. Another research group provided single crystal elastic constants for Fe-Mn-X (X=Al,Si) alloys from ab initio calculations [44]. Depending on the alloy composition, they found values of A ranging from 4.61 to 7.35.

If planar slip occurs on planes parallel to twin plane, twin boundaries do not reduce the mean free path of dislocations, since they do not act as barriers to dislocation motion parallel to them. If, in addition, single slip is at stake, the grains should display extended stage I hardening with small latent hardening due to low dislocation multiplication rate in other systems. Because of possible very high R values, situations even more characteristic as the classical $< 123 >$ orientation [46] could be expected. Hence, such grains should be very ductile. Moreover, their high plastic anisotropy should induce strong kinematic (directional) hardening by interactions with neighbouring grains (due to inter-granular incompatibility stresses) and large dislocations pile-ups at the grain boundary are very likely. As a consequence, the present results are consistent with the high ductility and strong kinematic hardening observed in TWIP steels [16]. As the deformation progresses and inter-granular incompatibility stresses develop, slip not parallel to twin plane will certainly occurs in most of the grains. As a result, twin boundaries will act as

obstacles for these additional systems. However, before accommodation between grains induces consequent inter-granular stresses, intra-granular stresses due to elastic mismatch between parent and twin phases should be predominant in grains where slip occurs parallel to twin plane. In the absence of plastic incompatibility inside these grains, the role of incompatibility stresses due to anisotropic elasticity is actually all the more important. Furthermore, it might be that twinned grains with very high R ratios (i.e., $R > 1.4$) show extended single slip behaviour despite the development of inter-granular stresses, compared to what happens in materials with twin-free grains and initial R values less than 1.38.

Besides, the fact that elastic anisotropy may promote planar slip on planes parallel to twin plane is also in full agreement with the widespread composite hardening models proposed for TWIP steels [20, 21]. According to these models, slip parallel to the most active twin plane is promoted in heavily twinned grains because twin boundaries hinder dislocation motion along other slip planes and planar slip is then accommodated by multislip in adjacent grains [20, 21]. This type of model is, in particular, recommended in order to capture the brass-type texture formation of TWIP steels [20, 21]. However, the model recently developed by Dancette et al. [20] failed to predict slip along a single plane inside individual grains, in spite of using a hardening law promoting slip parallel to the most active twin plane. On this issue, the present study therefore suggests that it may be worth considering also the contributions of intra-granular elastic incompatibility stresses between parent and twin phases.

Finally, it is worth also mentioning two recent works about the compression of copper bicrystalline micro pillars with $\Sigma 3 < 111 >$ twin boundaries [36, 47]. In both works, twin boundaries were parallel to the loading axis. Thus, there was no incompatibility stress due to elastic mismatch according to Equation 10 and a classical Schmid analysis revealed itself relevant to explain the slip initiation process. However, the results of the present paper show that the picture would have been completely different for a different orientation of the twin boundaries. Therefore, the present results should also be helpful for the design of new materials by grain boundary engineering methods using $\Sigma 3 < 111 >$ boundaries [15, 17].

8. Conclusion

In this paper, incompatibility stresses arising at general twin boundaries (type I or II) were, first, explicitly derived for a given twin volume fraction. Then, the case of $\Sigma 3 < 111 >$ twin boundaries present in f.c.c. structures was considered. In pure elasticity, the expression of the incompatibility stress field is of remarkable simplicity and just reduces to a shear stress acting upon a plane orthogonal to twin plane. Accordingly, a comprehensive study of slip initiation was performed for a lamellar $\Sigma 3 < 111 >$ twin structure. Depending on twin boundary orientation, elastic anisotropy factor and twin volume fraction, it was shown that slip and even single slip can be strongly promoted on planes parallel to twin plane, simultaneously in the parent and in the twin phases. The domains corresponding to the promotion of parallel simultaneous (single) slip displays quite realistic values if one considers the case of TWIP steels. Moreover, it must be noticed that single slip promotion can largely overcome the one corresponding to the best possible orientation for a single crystal in uniaxial loading. These results are thus fully consistent with the characteristics of TWIP steels, such as their high ductility and strong kinematic hardening [16], as well as their texture evolution which argues for a combination of single and multislip deforming grains [20, 21]. Finally, the significance of such simple expressions of incompatibility stresses for the design of new materials

with enhanced mechanical properties (e.g., strength, ductility, toughness) by twin boundary engineering methods [15, 17] must be underlined.

9. Acknowledgements

TR is grateful to the French National Research Agency (ANR) for financial support under contract "PHIRCILE" (ANR 2010 JCJC 0914 01). This work was also supported by the French State through the program "Investment in the future" operated by the National Research Agency (ANR) and referenced by ANR-11-LABX-0008-01 (LabEx DAMAS).

References

[1] N. Thompson and N. Wadsworth, Philos Mag A 1 (1956), p. 113.
[2] R. Boettner, A. McEvily, and Y. Liu, Philos Mag 10 (1963), p. 95.
[3] P. Neumann and A. Tönnessen, in *Proceedings of the 3rd International Conference on Fatigue and Fatigue Thresholds*, June, Charlottsville, U.S.A., 1987, p. 3.
[4] A. Heinz and P. Neumann, Acta Metall Mater 38 (1990), p. 1933.
[5] P. Gopalan and H. Margolin, Mat Sci Eng A 142 (1991), p. 11.
[6] C. Blochwitz and W. Tirschler, Mat Sci Eng A 339 (2003), p. 318.
[7] H. Ledbetter, Phys Stat Sol (a) 85 (1984), p. 89.
[8] Z. Zhang, P. Zhang, L. Li, and Z. Zhang, Acta Mater 61 (2012), p. 1383.
[9] H. Vehoff, A. Nykyforchyn, and R. Metz, Mat Sci Eng A 387-389 (2004), p. 546.
[10] A. Lewis and R. Kay, Metall Mater Trans A 39A (2008), p. 1109.
[11] J. Gemperlova, V. Paidar, and F. Kroupa, Czech J Phys B 39 (1989), p. 427.
[12] P. Peralta, L. Llanes, J. Bassani, and C. Laird, Philos Mag A 70 (1994), p. 219.
[13] P. Neumann, in *Proc of the 7th International Fatigue Congress*, June, Beijing, P.R.C., 1999, p. 107.
[14] T. Richeton and S. Berbenni, Eur J Mech A-Solids 37 (2013), p. 231.
[15] L. Lu, Y. Shen, X. Chen, L. Qian, and K. Lu, Science 304 (2004), p. 422.
[16] O. Bouaziz, S. Allain, and C. Scott, Scripta Mater 58 (2008), p. 484.
[17] Q. Pan, Q. Lu, and L. Lu, Acta Mater 61 (2013), p. 1383.
[18] S. Allain, Ph.D. thesis, Institut National Polytechnique de Lorraine, 2004.
[19] I. Gutierrez-Urrutia and D. Raabe, Acta Mater 59 (2011), p. 6449.
[20] S. Dancette, L. Delannay, K. Renard, M. Melchior, and P. Jacques, Acta Mater 60 (2012), p. 2135.
[21] T. Leffers and R. Kay, Prog Mat Sci 54 (2009), p. 351.
[22] W. Voigt, *Lehrbuch Der Kristallphysik*, B.G. Teubner, Leipzig, Germany, 1928.
[23] T. Richeton and S. Berbenni, Int J Solids Struct 51 (2014), p. 794.
[24] S. Stupkiewicz and H. Petrik, J Mech Phys Sol 50 (2002), p. 2303.
[25] P. Franciosi and S. Berbenni, J Mech Phys Solids 55 (2007), p. 2265.
[26] C. Rey and G. Saada, Philos Mag 33 (1976), p. 825.
[27] C. Rey and A. Zaoui, Acta Metall 28 (1980), p. 711.
[28] P. Peralta and C. Laird, Acta Mater 70 (1997), p. 219.
[29] P. Peralta, A. Schober, and C. Laird, Mat Sci Eng A 169 (1993), p. 43.
[30] A.E. Omri, A. Fennan, F. Sidoroff, and A. Hihi, Eur J Mech A-Solids 19 (2000), p. 585.
[31] J.W. Christian and S. Mahajan, Prog Mater Sci 39 (1995), p. 1.
[32] E. Schmid and W. Boas, *Kristallplasticität*, Springer Verlag, Berlin, 1935.
[33] T. Richeton, C. Schuman, J. Lecomte, L. Bao, and C. Fressengeas, Int J Solids Struct 49 (2012), p. 1355.
[34] Y. Zhu, X. Wu, X. Liao, J. Narayan, L. Kecskes, and S. Mathaudhu, Acta Mater 59 (2011), p. 812.
[35] Y. Zhu, X. Liao, and X. Wu, Prog Mater Sci 57 (2012), p. 1.
[36] L. Li, X. An, P. Imrich, P. Zhang, Z. Zhang, G. Dehm, and Z. Zhang, Acta Mater 69 (2013), p. 199.
[37] M. Ortiz and E. Repetto, J Mech Phys Solids 47 (1999), p. 397.
[38] L. Rémy, Acta Metall 25 (1976), p. 825.
[39] T. Takeuchi, Trans. JIM 16 (1975), p. 629.

[40] J. Finney, Ph.D. thesis, University of Pennsylvania, Philadelphia, Pennsylvania, 1974.
[41] D. Barbier, N. Gey, S. Allain, N. Bozzolo, and M. Humbert, Mat Sci Eng A 500 (2009), p. 196.
[42] O. Bouaziz, S. Allain, C. Scott, P. Cugy, and D. Barbier, Curr Opin Solid St M 15 (2011), p. 141.
[43] D. Pierce, K. Nowag, A. Montagne, J. Jimnez, J. Wittig, and R. Ghisleni, Mat Sci Eng A 578 (2013), p. 134.
[44] T. Gebhardt, D. Music, D. Kossmann, M. Ekholm, I. Abrikosov, L. Vitos, and J. Schneider, Acta Mater 59 (2011), p. 3145.
[45] R. Fullman, Trans AIME 197 (1953), p. 447.
[46] L. Kubin, B. Devincre, and T. Hoc, Acta Mater 56 (2008), p. 6040.
[47] T. Hirouchi and Y. Shibutani, Mater Trans JIM 55 (2014), p. 52.